The use of the TCNQF$_4$$^{2-}$dianion in the spontaneous redox formation of [Fe^{III}(L$^-$)$_2$][TCNQF$_4$$^{•-}$] .[#],[*]

Ian A. Gass,*[a][b] Jinzhen Lu,[a] Mousa Asadi,[a] David W. Lupton,[a] Craig. M. Forsyth,[b] Blaise L. Geoghegan,[b] Boujemaa Moubaraki,[a] John D. Cashion,[c] Lisandra L. Martin,[a] Alan M. Bond,[a] and Keith S. Murray*[a]

Abstract: The reaction of [Fe^{II}(L$^•$)$_2$](BF$_4$)$_2$ with Li$_2$TCNQF$_4$ results in the formation of [Fe^{III}(L$^-$)$_2$][TCNQF$_4$$^{•-}$] (**1**) where L$^•$ is the radical ligand, 4,4-dimethyl-2,2-di(2-pyridyl)oxazolidine-N-oxide and TCNQF4 is 2,3,5,6-Tetrafluoro-7,7,8,8-tetracyano-quinodimethane. This has been characterised by x-ray diffraction, Raman and Fourier-transform infra-red (FTIR) spectroscopy, variable temperature magnetic susceptibility, Mössbauer spectroscopy and electrochemistry. X-ray diffraction studies, magnetic susceptibility measurements and Raman and FTIR spectroscopy suggest the presence of low-spin Fe^{III} ion, the anionic form (L$^-$) of the ligand and the anionic radical form of TCNQF$_4$; TCNQF$_4$$^{•-}$. Li$_2$TCNQF$_4$ reduces the [Fe^{II}(L$^•$)$_2$]$^{2+}$ dication which undergoes a reductively induced oxidation to form the [Fe^{III}(L$^-$)$_2$]$^+$ monocation resulting in the formation of [Fe^{III}(L$^-$)$_2$][TCNQF$_4$$^{•-}$] (**1**), the electrochemistry of which revealed four well-separated, diffusion controlled, one-electron, reversible processes. Mössbauer spectroscopy and electrochemical measurements suggest the presence of a minor second species, likely to be [Fe^{II}(L$^•$)$_2$][TCNQF$_4$$^{2-}$].
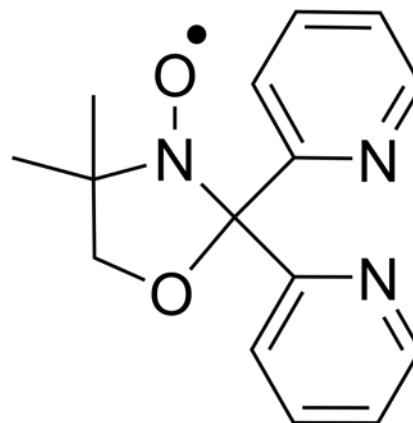
Figure 1. Structural formula of 4-dimethyl-2,2-di(2-pyridyl) oxazolidine-N-oxide (L$^•$)

Introduction

Multifunctional materials are constructed from a simple ethos in which at least two species, with differing physical and electronic properties are combined to give a new material which on the basis of synergistic interactions exhibits either improved or modified physical properties or, in some cases, gives rise to entirely new phenomena.[1–10] An obvious strategy to achieve this goal is to combine cation / anion pairs with desirable properties and use this "salt" formation as the driving force to prepare new materials. Recent examples of multifunctional magnetic materials prepared by this strategy include: [Fe^{II}(tren(imid)$_3$)]$_2$[Mn^{II}Cl$_2$Cr^{III}(Cl$_2$An)$_3$]Cl which exhibits long-range magnetic ordering below 2.6 K and an incomplete, gradual spin transition from 100 K to 280 K;[11] [Fe^{III}(qnal)$_2$]$_n$rGO which shows both electrical conductivity and spin-crossover behavior (Hqnal = (1-((8-quinolinylimino)methyl)-2- naphthalenol , rGO = reduced graphene oxide);[12] and [Fe^{III}(Iqsal)$_2$][Ni(dmit)$_2$]

where there is clear evidence of the synergy between the halogen bond stabilized spin-Peierls like singlet formation of the [Ni(dmit)$_2$] anions and the abrupt spin-transition at 150 K[13] (tren(imid)$_3$ = tris(2-(((Z)-(1H-imidazol-4-yl)methylene)amino)ethyl)amine; Cl$_2$An = 2,5-dichloro-3,6-dioxocyclohexa-1,4-diene-1,4-bis(olate); Hqnal = (1-((8-quinolinylimino)methyl)-2-naphthalenol; rGO = reduced graphene oxide; HIqsal=5-iodo-N-(8'-quinolyl)-salicylaldinine and dmit = 4,5-dithiolato-1,3-dithiole-2-thione). In these examples, the cation of choice was a spin-crossover moiety but this could easily be substituted for one with single-molecule magnet (SMM),[14] luminescent,[15] or redox-active behaviour.[16]

The recently reported redox congeners [Fe^{II}(L$^•$)$_2$][BF$_4$]$_2$ and [Fe^{III}(L$^-$)$_2$](BPh)$_4$[17,18] (L$^•$ = 4-dimethyl-2,2-di(2-pyridyl)oxazolidine-N-oxide) display multistep redox processes and in effect represent a switchable system in which the diamagnetic [Fe^{II}(L$^•$)$_2$]$^{2+}$ dication can be inter-converted to the paramagnetic [Fe^{III}(L$^-$)$_2$]$^+$ species via electrochemical or chemical means. The cobalt analogues are represented by the dication, [Co^{II}(L$^•$)$_2$]$^{2+}$ and monocation [Co^{III}(L$^-$)$_2$]$^+$ which exhibit similar redox processes to the iron complexes above as well as host of other interesting properties such as solvate dependent exchange / spin-crossover and single-molecule magnet (SMM) like behaviour.[19,20] In the cobalt case the S = 3/2 [Co^{II}(L$^•$)$_2$]$^{2+}$ dication could be interconverted to the diamagnetic [Co^{III}(L$^-$)$_2$]$^+$ monocation. The manganese analogue, [Mn^{II}(L$^•$)$_2$](ClO$_4^-$)$_2$, can in principle undergo similar redox chemistry but some reactions are of an irreversible nature.[21]

Clearly an attractive choice for generation of multi-functional magnetic materials could be based on combining cations containing the L$^•$/ L$^-$ ligand system and suitable redox-active anions. In this context we now propose that the [M^{II}(L$^•$)$_2$]$^{2+}$ /

[a] Dr I. A. Gass, Dr J. Lu, Dr M. Asadi, Assoc. Prof. D.W. Lupton, Dr. C. M. Forsyth, Dr B. Moubaraki, Assoc. Prof. L. L. Martin, Prof. A. M. Bond, Prof. K. S. Murray
School of Chemistry, Monash University, Clayton, Victoria 3800
E-mail: Keith.Murray@monash.edu
[b] Dr I. A. Gass, Mr B. L. Geoghegan
School of Pharmacy and Biomolecular Sciences, University of Brighton, Brighton BN2 4GJ, UK E-mail: I.Gass@brighton.ac.uk
[c] Assoc. Prof. J. D. Cashion
School of Physics and Astronomy, Monash University, Clayton, Victoria 3800, Australia
Supporting information for this article is given via a link at the end of the document

L- = anionic form of 4,4-dimethyl-2,2-di(2-pyridyl)oxazolidine-N-oxide.
*In memory of Leone Spiccia

[M^{III}(L$^-$)$_2$]$^+$ (M = Fe, Co) class of redox congener cations can replace tetrathiafulvalene (TTF) analogues in the archetypal charge transfer complex TTF-TCNQ.[22] Here we report on the synthesis of [Fe^{III}(L$^-$)$_2$][TCNQF$_4$$^{•-}$] (**1**) The paramagnetic species, **1**, is formed by a spontaneous redox formation using TCNQF$_4$$^{2-}$, derived from Li$_2$TCNQF$_4$, as a reducing agent to convert the dication in [Fe^{II}(L$^•$)$_2$][BF$_4$]$_2$ to the [Fe^{III}(L$^-$)$_2$]$^+$ monocation via a reductively induced oxidation reaction.[17,18] During this process TCNQF$_4$$^{2-}$ is oxidized to TCNQF$_4$$^{•-}$ which provides the necessary charge balance to the resultant [Fe^{III}(L$^-$)]$^+$ monocation. This results in a paramagnetic material, [Fe^{III}(L$^-$)$_2$][TCNQF$_4$$^{•-}$] (**1**), synthesized from two diamagnetic starting materials. Recently, Dunbar et al. have reported the synthesis of [Co^{II}(terpy)$_2$](TCNQ)$_3$.CH$_3$CN (terpy = 2,2';6',2"-terpyridine and TCNQ = 7,7,8,8-tetracyanoquino-dimethane) which displays hybrid properties of spin crossover and an anomaly in its solid state conductance, the latter originating from the partially charged TCNQ in the dianionic triad [(TCNQ)(TCNQ$^•$)$_2$]$^{2-}$.[23]

Results and Discussion

Synthesis and Solid State Structures

The [Fe^{II}(L$^•$)$_2$]$^{2+}$ dication is known to undergo a reductively induced oxidation of the central Fe^{II} metal ion by reaction with the tetraphenylborate (Ph$_4$B$^-$) anion resulting in the formation of the [Fe^{III}(L$^-$)$_2$]$^+$ monocation[17,18]. A related redox process would be expected to occur when using TCNQF$_4$$^{2-}$ as the reductant.[24] In this case TCNQF$_4$$^{2-}$ is likely to be oxidised to the TCNQF$_4$$^{•-}$ radical anion and in the process, via an intramolecular electron transfer, the [Fe^{III}(L$^-$)$_2$]$^+$ monocation would be formed from [Fe^{II}(L$^•$)$_2$]$^{2+}$ via a reductively induced oxidation. This redox chemistry would have the overall effect of producing two paramagnetic species from two diamagnetic components via an intermolecular electron transfer. Pleasingly, layering one equivalent of a methanolic solution of freshly prepared Li$_2$TCNQF$_4$ on a solution of [Fe^{II}(L$^•$)$_2$][BF$_4$]$_2$[17] in a mixture of acetonitrile and dichloromethane resulted in the formation of crystalline [Fe^{III}(L$^-$)$_2$][TCNQF$_4$$^{•-}$] (**1**) in 59% yield.

1 crystallizes in the triclinic space group ==P̄1== with the asymmetric unit containing half the [Fe^{III}(L$^-$)$_2$]$^+$ monocation and half the [TCNQF$_4$]$^{•-}$ radical monoanion. Structural features of **1** are provided in Figure 2 and relevant bond lengths and angles can be found in Tables 1 and 2. An inversion centre sits on the central iron ions in **1** generating the monocation [Fe^{III}(L$^-$)$_2$]$^+$. Single crystal X-ray diffraction studies enabled us to tentatively identify the oxidation states and spin states of the iron in the cationic species [Fe$^{II/III}$(L$^{•/-}$)$_2$]$^{2+/+}$, the redox level of the TCNQF$_4$ moieties in **1** and the neutral radical (L$^•$) or hydroxylamino form (L$^-$) of the ligand via examination of the relevant bond lengths and angles (Tables 1, 2 and 3). This initial assignment of the relevant spin/oxidation states of the species contained within **1** is confirmed by variable temperature magnetic susceptibility measurements, the Mössbauer effect, UV-Visible, infrared and Raman spectroscopies, as well as electrochemical measurements.
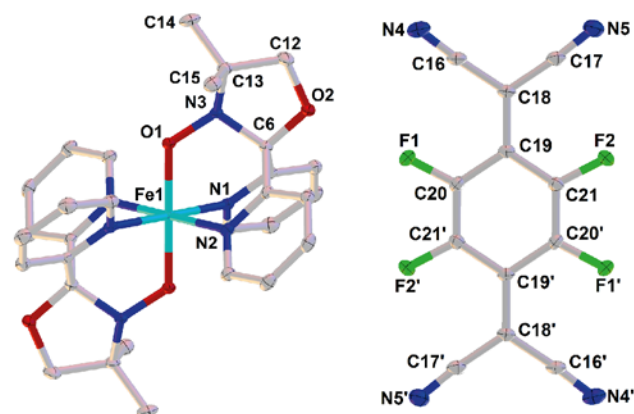

Figure 2. Molecular structure of the monocation [Fe^{III}(L$^-$)$_2$]$^+$ of **1** (left) and TCNQF$_4$$^{•-}$ radical anion in **1** (right).

In **1** the tridentate nitroxide radical ligand coordinates to the Fe ion axially via the oxygen and equatorially via the pyridyl nitrogen groups resulting in a distorted octahedral geometry (Figure 2) (complex **1**: cis angles, 86.08(6) – 93.92(9)°;

Table 1. Selected bond lengths (Å) and angles (°) for the monocation [Fe^{III}(L$^-$)$_2$]$^+$ in 1.

	[Fe^{III}(L$^-$)$_2$]$^+$ in **1**
O(1)-N(3)	1.4177(19)
Fe(1)-O(1)	1.8551(12)
Fe(1)-N(1)	1.9869(16)
Fe(1)-N(2)	1.9553(15)
N(3)-C(6)	1.479(2)
N(3)-C(13)	1.490(2)
C(6)-O(2)	1.403(2)
O(2)-C(12)	1.447(2)
C(12)-C(13)	1.527(3)
C(13)-C(14)	1.524(3)
C(13)-C(15)	1.531(3)
Fe(1)-O(1)-N(3)	117.12(9)
Fe(1)-O(1)-N(3)-C(6)[a]	-31.917
Fe(1)-O(1)-N(3)-C(13)[a]	-151.101
O(1)-N(3)-C(6)-C(13)[a]	-123.114

[a] For a system with four atoms A, B, C, D the torsion angle A-B-C-D will be the angle formed between the plane formed by A, B and C and the plane formed between B, C and D. The sign of the torsion angle is positive if the bond A-B is rotated in a clockwise direction through less than 180° in order that it may eclipse the bond C-D: a negative torsion angle requires rotation in the opposite sense.

Table 2. Selected bond lengths (Å) and angles (°) for the anionic radical $[TCNQF_4]^{\bullet-}$ in **1**.

	$[TCNQF_4]^{\bullet-}$ in **1**
N(4)-C(16)	1.145(3)
N(5)-C(17)	1.147(3)
C(16)-C(18)	1.428(3)
C(17)-C(18)	1.425(3)
C(18)-C(19)	1.419(2)
C(19)-C(20)	1.416(3)
C(19)-C(21)	1.416(3)
C(20)-C(21')	1.365(3)
C(21)-C(20')	1.365(3)
F(1)-C(20)	1.345(2)
F(2)-C(21)	1.346(2)

trans angles, all 180°; Fe-O 1.8551(12) Å, Fe-N 1.9869(16), 1.9553(15) Å; The intramolecular (L⁻ to L⁻) distance in **1** is 4.536 Å In both cases this intramolecular distance was made between calculated centroids of the nitroxide N-O group. The $TCNQF_4^{\bullet-}$ radical anion is non-coordinating with one $TCNQF_4^{\bullet-}$ radical anion present per $[Fe^{III}(L^-)_2]^+$ monocation (Figure 2).

The redox chemistry of both the neutral radical (L•) and $TCNQF_4$ are summarized in Scheme 1. The crystallographic bond lengths and angles (Tables 1 and 2) are used to assign the redox level of the tridentate ligand and $TCNQF_4$. For the cationic Fe species in **1**, the nitroxide N-O (N3-O1) bond length is 1.4177(19) Å which is clearly appropriate for the hydroxylamino anionic form of the ligand (L⁻).[17–21] The Fe-O (1.8551(12) Å) and Fe-N (1.9869(16) and 1.9553(15) Å) bond lengths are consistent with earlier studies on $[Fe^{III}(L^-)_2](BPh_4)$[17,18] so we can confidently assign the cationic species as $[Fe^{III}(L^-)]^+$ where the Fe^{III} ion is low-spin. Further evidence for this assignment is provided by the torsion angle O1-N3-C6-C13 of -123.114° (Table 1 and Figure 3) indicating deviation from the plane formed by O1-C6-C13 (Figure 3). The trigonal pyramidal geometry around N3 is strongly suggestive of a localized lone pair which is expected for the ligand in the hydroxylamino anionic form, L⁻ (Figure 3). The above arguments detailed in Figure 3, represent a valence bond theory approach, appropriate in this case as a reasonable explanation of the geometry around N3 is provided and agreement is achieved with the molecular orbital diagrams reported previously for $[Fe^{III}(L^-)_2](BPh_4)$ and $[Fe^{II}(L^\bullet)_2](BF_4)_2$.[17]

The cationic species are therefore assigned as $[Fe^{III}(L^-)_2]^+$ (where the Fe^{III} ion is low-spin) in **1**.

From charge balance considerations alone, the $TCNQF_4$ species in **1** must be the anionic radical form, $TCNQF_4^{\bullet-}$. Confirming the correct spin/oxidation states for $TCNQF_4$ can be

achieved by a formal analysis of the bond lengths (Table 3). As changes from
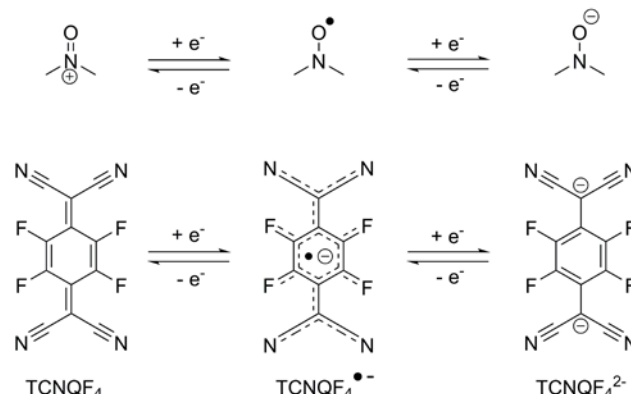
Scheme 1. Schematic representation of the nitrosonium cation (top left), neutral nitroxide radical (top middle), hydroxylamine anion (top right), neutral $TCNQF_4$ (bottom left), $TCNQF_4^{\bullet-}$ radical anion (bottom middle) and dianionic $TCNQF_4^{2-}$ (bottom right).

Figure 3. The deviation from the plane formed by O(1)-C(6)-C(13) and a
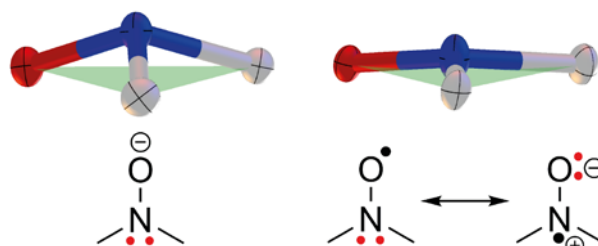
sketch of the location of the both the unpaired electron and the lone pair in the nitroxide N-O group in complex 1, $[Fe^{III}(L^-)_2][TCNQF_4•-]$, (left) and $[Fe^{II}(L•)_2](BF_4)_2$ (right).[14]

Table 3. Calculation of the charge transfer degree ρ using C-C and C=C mean bond lengths; b,c and d as designated below.

Material	b	c	d	ρ [a]
1	1.416	1.419	1.427	-0.99
$[TCNQF_4]$	1.437	1.372	1.437	0
$(n\text{-Bu}_4N)[TCNQF_4]^{\bullet-}$	1.417	1.418	1.426	-1.00
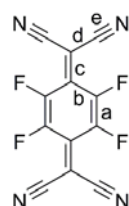
[a] $\rho = A(c/(b+d)) + B$ where A = -45.756 and B = 21.846 which are calculated from $[TCNQF_4]$ and $[TCNQF_4]•-$ assuming $\rho = 0$ for the neutral $[TCNQF_4]$ moiety and $\rho = -1$ for the anionic radical form in $[TCNQF_4]•-$. The values in Table 3 are taken from $TCNQF_4$[25] and (n-Bu₄N)[TCNQF₄]•-.[26] Average values are used when there are two crystallographically independent but chemically equivalent bond lengths.

the neutral $TCNQF_4$ form to the monoanionic radical form and then on to the dianionic aromatic form occur, the bond length labelled c (Scheme 1 and Table 3) increases in length while b and d decrease. The charge transfer degree of the $TCNQF_4$ moiety (ρ) can be estimated from the Kistenmacher relationship[25] (Table 3). The calculated ρ values are -0.99 for **1**, confirming that the $TCNQF_4$ moiety in **1** is of the $TCNQF_4^{\bullet-}$ radical anion form. **1** is therefore further confirmed as $[Fe^{III}(L^-)_2][TCNQF_4^{\bullet-}]$.

The crystal structure of **1** consists of alternating layers of $[Fe^{III}(L^-)_2]^+$ and $[TCNQF_4]^{\bullet-}$ (Figure 4) with no significant intermolecular interactions being noted. The shortest intermolecular distances are 8.079 Å (Fe to Fe), 5.564 Å (L^- to L^-) and 6.555 Å (Fe to L^-) where distances involving L^- were based on calculated centroids of the nitroxide N-O group. The interplanar distance between neighboring $TCNQF_4^{\bullet-}$ groups is 3.367 Å which equates to the distance between calculated centroids of the plane formed by N4-C16-C18-C17-N5 (Figure 2).

Figure 4. Packing diagram of 1 showing the arrangement of $[Fe^{III}(L^-)_2]^+$

monocations and $[TCNQF_4]^{\bullet-}$ radical anions.
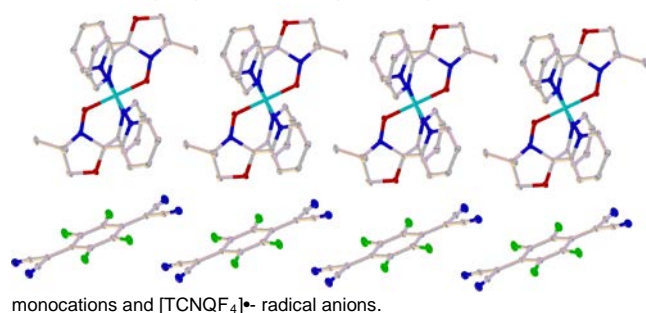
The packing arrangement of the $TCNQF_4^{\bullet-}$ groups in **1** (Figure 5) differs from that found in $[Pr_4N][TCNQF_4^{\bullet-}]$,[24] [$n$-$Bu_4N][TCNQF_4^{\bullet-}]$ ($P2_1/n$ collection),[26] [EDO-TTF-$CONH_2][TCNQF_4^{\bullet-}]$,[27] $[[W(\eta-C_5H_4Bu^t)_2(C_3S_5)][TCNQF_4^{\bullet-}]$[28] , [1-methylquinolinium][$TCNQF_4^{\bullet-}$][29] and [triethyl(3-nitrobenzyl)ammonium][$TCNQF_4^{\bullet-}$][29] which all form eclipsed or stacked face-to-face dimers (EDO-TTF-$CONH_2$ = (ethylenedioxo)-carbamoyltetrathiafulvalene and $C_3S_5^{2-}$ = 4,5-disulfanyl-1,3-dithiole-2-thionate). A ring-over-bond stepped arrangement forms in the analogous compound, [HSTMF][$TCNQF_4^{\bullet-}$][30]; a 1D column containing ring-over bond dimers occurs in $[BuGH^+][[TCNQF_4^{\bullet-}]$[31]; and [CpMo(SMe)$_4$MoCp][$TCNQF_4^{\bullet-}$][32] shows a crosswide mode overlap between the [$TCNQF_4^{\bullet-}$] anions (HSTMF = Hexamethylenetetra-selenafulvalene and $BuGH^+$ = protonated 9-n-butylguanine). The closest conformation to that observed in **1** is present in [n-$Bu_4N][TCNQF_4^{\bullet-}]$[26] ($P\bar{1}$ collection) and a similarly loose association can be found between $TCNQF_4^{\bullet-}$] anions when the cation, 8-(dimethylamino)-N,N-dimethylnapthalen-1-aminium, is used.[29]

Raman and FT-IR spectroscopy

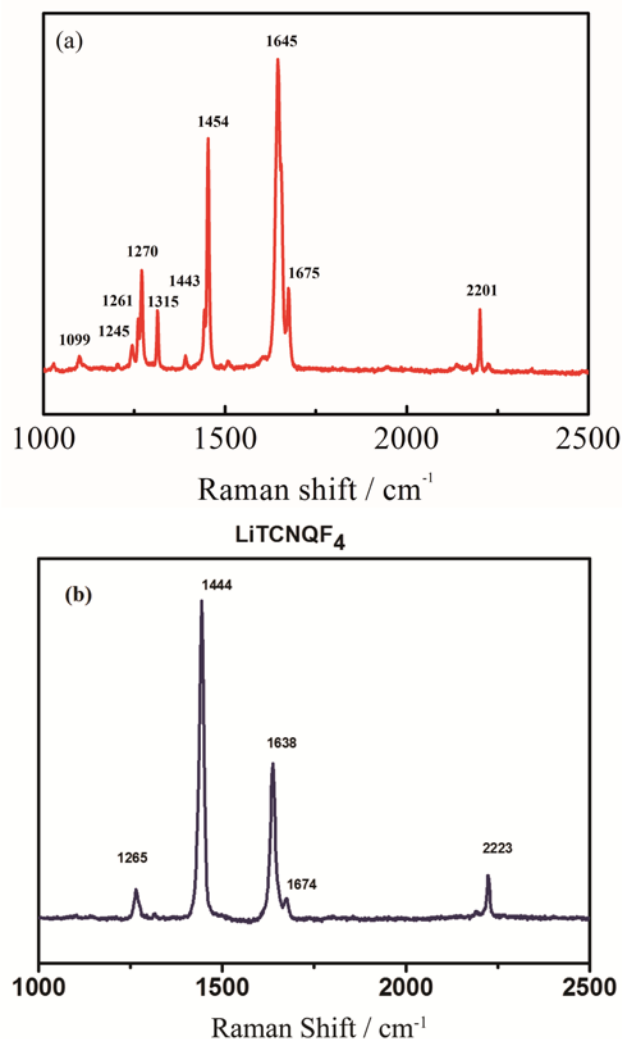Raman and Infrared spectroscopic data have been used to assist in the assignment of the 0, 1- or 2- redox level in

Figure 5. Raman spectra for (a) **1** and (b) LiTCNQF$_4$

$TCNQF_4^{0/1-/2-}$ and $TCNQ^{0/1-//2-}$ materials.[33,34] In the case of $TCNQF_4$ materials, density functional theory has been introduced to assist in distinguishing vibrational spectroscopic data for the $TCNQF_4$, $TCNQF_4^-$ and $TCNQF_4^{2-}$ redox levels. The most important diagnostic Raman band is associated[25] with the C≡N stretch and is located at 2226 cm^{-1} for solid neutral $TCNQF_4$.[35] By comparison, this vibrational mode is observed at 2201 cm^{-1} for **1** (Figure 5a). This is shifted to lower energies compared to neutral $TCNQF_4$ and in this context is consistent with the expectation for the $TCNQF_4^{\bullet-}$ radical anion.[24,26,33] where the C≡N band in LiTCNQF$_4$ is located at 2223 cm^{-1} (Figure 5b) and at 2205 cm^{-1} for (Pr$_4$N)TCNQF$_4$, similar to that observed in **1**. The equivalent C≡N band in Li$_2$TCNQF$_4$ is located at 2119 cm^{-1}. [21]

The FTIR spectrum for **1** is shown in Figure S3 in the Supporting Information and the C≡N stretches are observed at 2194 and 2174 cm^{-1} for **1**. On the basis of Raman and IR vibrational spectroscopic data alone[24] it would be difficult to detect a small amount of $TCNQF_4^{2-}$ or other $TCNQF_4^{\bullet-}$ based material that

might be present in **1** and would require analysis of the bulk solid samples by other techniques (*vide infra*).
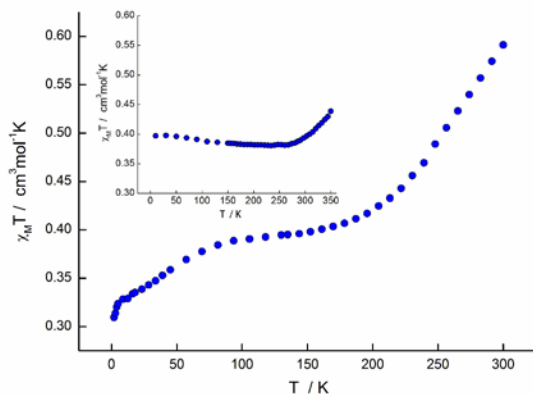
Magnetic Studies

Figure 6. Plot of $\chi_M T$ vs T for 1 (main) and for $[Fe^{III}(L^-)_2][BPh_4]$ (inset).

DC magnetic susceptibilities were performed on bulk crystals of **1** in the 2 to 300 K range under an applied field of 1.0 T (Figure 6). The $\chi_M T$ value of 0.59 cm³ mol⁻¹ K at 300 K decreases rapidly upon cooling to a $\chi_M T$ value of 0.40 cm³ mol⁻¹ K at 160 K which then forms a plateau down to 106 K (Figure 6). The $\chi_M T$ value then decreases linearly upon cooling reaching a $\chi_M T$ value of 0.33 cm³ mol⁻¹ K at 12.3 K followed by a sharp reduction in the $\chi_M T$ values finally reaching a $\chi_M T$ value of 0.31 cm³ mol⁻¹ K at 2 K, the latter reduction presumably due to Zeeman depopulation effects. The $\chi_M T$ value of 0.59 cm³ mol⁻¹ K at 300 K is slightly lower than the expected value from the sum of the contribution from the low-spin Fe(III) ion (~ 0.40 cm³ mol⁻¹ K)[1] and the unpaired radical electron on the $[TCNQF_4]^{•-}$ radical anion (0.375 cm³ mol⁻¹ K) indicating some degree of antiferromagnetic exchange. The $\chi_M T$ value given above for the expected contribution from the low-spin Fe(III) ion of 0.40 cm³ mol⁻¹ K was based on the $\chi_M T$ vs T data for the previously reported $[Fe^{III}(L^-)_2][BPh_4]$[17] (Figure 6 inset). Both $[Fe^{III}(L^-)_2][BPh_4]$[17] (Figure 6 inset) and **1** (Figure 6 main) share a sharp rise in the $\chi_M T$ values at higher temperatures. The two possible contributions to the sharp rise in the $\chi_M T$ values between 160 and 300 K are: (a) the $[TCNQF_4]^{•-}$ radical anions are coupled antiferromagnetically to each other with residual contributions from the $[Fe^{III}(L^-)_2]^+$ monocation and; (b) the $[TCNQF_4]^{•-}$ radical anions are strongly antiferromagnetically coupled to each other and the $[Fe^{III}(L^-)_2]^+$ monocation undergoes a gradual incomplete thermally activated spin crossover above 160 K. It is reasonable to suggest that the $[TCNQF_4]^{•-}$ radical anions in the stepped conformation seen in Figure 4 can undergo an observable antiferromagnetic exchange coupling when the related compound with a similar conformation <mark>present</mark>, [*n*-Bu₄N][TCNQF₄] (<mark>*P1̄*</mark> collection),[26] shows a triplet state (S =1) which is thermally accessible below 300 K. This is in stark contrast to the diamagnetic behavior typical of eclipsed or

stacked $[TCNQF_4]^{•-}$ radical anion pairs.[36],[37],[38] It is possible the rise in the $\chi_M T$ values above 160 K could be solely due to an incomplete d⁵ spin-crossover transition but this would correspond to ~5% HS and 95% LS at 300 K and would require very strong π-π antiferromagnetic coupling between the $[TCNQF_4]^{•-}$ anions to obtain a $\chi_M T$ value of 0.59 cm³ mol⁻¹ K; unlikely given the stepped conformation of the $[TCNQF_4]^{•-}$ radical anions in **1** as discussed above. It is more likely due to a combination of weakly antiferromagnetically coupled $[TCNQF_4]^{•-}$ radical anions and some temperature dependent contribution from the $[Fe^{III}(L^-)_2]^+$ monocation. The shape of the rise in the $\chi_M T$ values from above 160 K does not seem appropriate for a simple temperature dependent plot we would expect from the ²T$_{2g}$ term of low-spin Fe(III)[39] but it is interesting to note that both **1** and $[Fe^{III}(L^-)_2][BPh_4]$[17] show this rise in the $\chi_M T$ values (Figure 6) at higher temperatures indicating that the origin is, at least in part, due to a contribution from the $[Fe^{III}(L^-)_2]^+$ monocation.

The central plateau $\chi_M T$ values of around 0.40 cm³ mol⁻¹ K between 106 K and 160K are consistent with the values expected from the contribution of the low-spin Fe(III) ion (~ 0.40 cm³ mol⁻¹ K)[17] in the $[Fe^{III}(L^-)_2]^+$ monocation. The monotonic decrease in the $\chi_M T$ values below 106 K are surprising given the expectation for a low-spin Fe(III) ion and are not due to torqueing effects since the sample was dispersed in Vaseline. There is no evidence for any antiferromagnetic ordering or any dependence of the molar magnetic susceptibility on the magnetic field strength at low temperatures to account for the monotonic decrease in the $\chi_M T$ values below 106 K (Figure 7).

Mössbauer spectroscopic measurements on **1** (*vide infra*) shown in Figure 8 suggests the presence of a minor second species and so any contribution this may have on the $\chi_M T$ vs T plots needs to be considered**.** This would most likely be the $[Fe^{II}(L^•)(L^-)]^+$ monocation or a species containing the $[Fe^{II}(L^•)_2]^{2+}$ dication, potentially with diamagnetic $TCNQF_4^{2-}$ as the anion . The $[Fe^{II}(L^•)(L^-)]^+$ monocation would be expected to contain a low-spin Fe^{II} ion consistent with previous studies[17] and a single unpaired electron from the neutral radical ligand and therefore would not account for the monotonic decrease in the $\chi_M T$ values below 106 K. The $[Fe^{II}(L^•)_2]^{2+}$ dication[1] undergoes a strong antiferromagnetic coupling between the two radicals via the low-spin(II) centre and subsequently has a rise in the $\chi_M T$ values from ~0.01 cm³ mol⁻¹ K at 100K to 0.16 cm³ mol⁻¹ K at 300 K and is largely diamagnetic below 100 K. A small percentage of the $[Fe^{II}(L^•)_2]^{2+}$ dication may account for the decrease in the $\chi_M T$ values at lower temperature especially considering the drop in the $\chi_M T$ values in complex **1** from 0.40 cm³ mol⁻¹ K at 160K to 0.33 cm³ mol⁻¹ K at 12 K is around a 20% reduction, consistent with the presence of 19% of a second, and diamagnetic below 100 K, minor species. This would also decrease the $\chi_M T$ values at higher temperatures compared to those expected for the presence of 100% of complex **1**. The $[Fe^{II}(L^•)_2]^{2+}$ dication could be present as either $[Fe^{II}(L^•)_2][TCNQF_4]$ $[Fe^{II}(L^•)_2](BF_4)_2$[17] or $[Fe^{II}(L^•)_2][TCNQF_4^{•-}]_2$. The second species could also conceivably be $[(Fe^{III}(L^-)_2)_2](TCNQF_4^{2-})$ although the currently reported Mössbauer parameters for the second species (*vide infra*) are significantly different to those obtained for
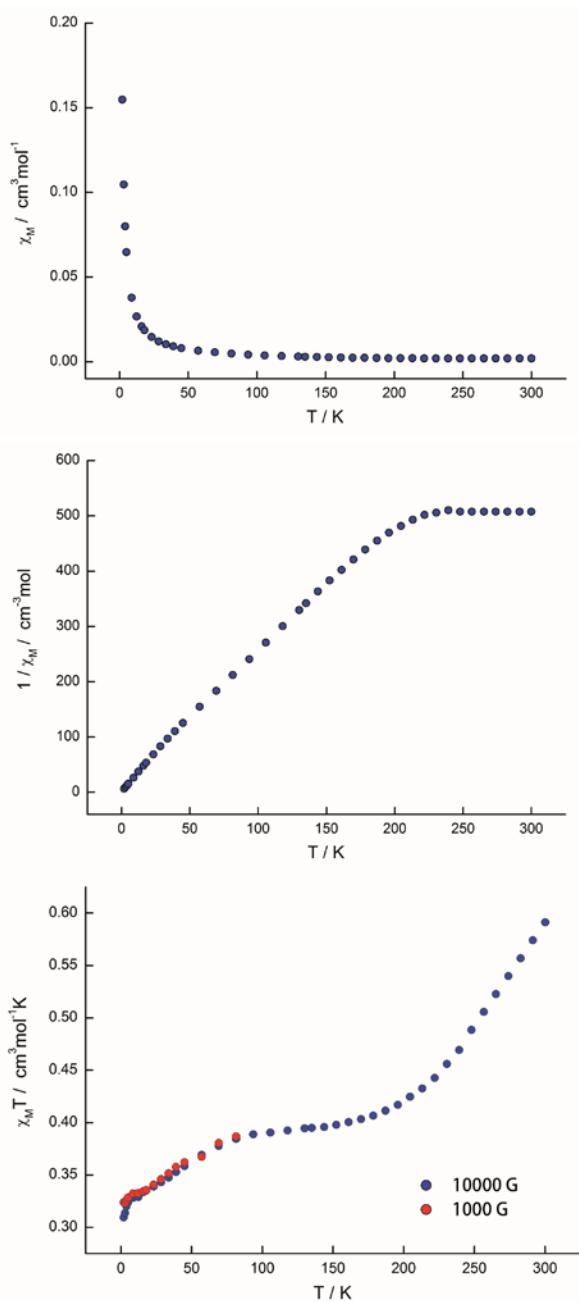
Figure 7. Plot of χ_M vs T (top left), $1/\chi_M$ vs T (top right) and $\chi_M T$ vs T at 10000 G (blue circles) and 1000 G (red circles) (bottom) for **1**.

[Fe^{III}(L$^-$)$_2$](BPh)$_4$[17] where the central Fe(III) ion is low-spin. A high-spin variant of [(Fe^{III}(L$^-$)$_2$)$_2$](TCNQF$_4$$^{2-}$) would be expected to have similar Mössbauer parameters to those reported for the second minor species but this does not account for the magnitude and monotonic decrease of the $\chi_M T$ values below 106 K.

Mössbauer Spectroscopy

In order to seek spectroscopic verification of the presence of any second species in the bulk solid of **1** that contributes to the magnetism, Mössbauer spectra and XRD powder patterns were obtained on the same material used in the magnetic studies.
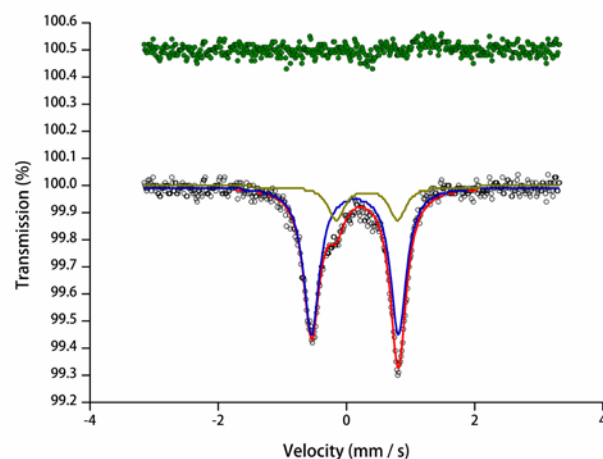

Figure 8. Zero field ^{57}Fe Mössbauer spectra of 1 at 300 K showing the best-fit to two Voigtian doublets as a red line and the constituent quadrupole doublets as blue and green lines. Velocity scale relative to metallic iron. The top green points are the difference between the data and the fit.

Table 4. Fitted parameters to the Mössbauer Spectrum of [Fe^{III}(L$^-$)$_2$][TCNQF$_4$•-] (**1**) at room temperature ($\chi^2 = 0.52$).

c	QS (mm/s)	Linewidth (mm/s)	Area (%)
0.13(2)	1.36(5)	0.30	81
0.34(10)	0.96(20)	0.36	19

The Mössbauer spectrum of **1**, at room temperature, is shown in Figure 8 as an asymmetric doublet with a shoulder on the low velocity component. The lineshape can be fitted adequately to two quadrupole split doublets. The isomer shift (IS) and quadrupole splitting (QS) of the main doublet are typical of low-spin Fe(III) and very similar to those of [Fe^{III}(L$^-$)$_2$](BPh$_4$).0.5H$_2$O.[17] The second doublet has parameters very similar to that of [Fe^{II}(L$^•$)$_2$][BF$_4$]$_2$[17] which contains a central low-spin Fe(II) ion and hence is unlikely to be due to a high-spin form of [Fe^{III}(L$^-$)$_2$][TCNQF$_4$$^{•-}$] (**1**). Although low-spin Fe(II) ions and high-spin Fe(III) ions have similar Mössbauer parameters the monotonic decrease of the $\chi_M T$ values below 106 K does not seem appropriate for a system which is purely [Fe^{III}(L$^-$)$_2$][TCNQF$_4$$^{•-}$] undergoing a gradual spin-crossover transition. Additionally the rise in the $\chi_M T$ values above 160 K is highly likely due to an observable antiferromagnetic coupling between the [TCNQF$_4$]$^{•-}$ radical anions. The small misfit at approximately 0.3 mm/s could not be unambiguously fitted and two alternative possible interpretations with a third spectral component are given in the supporting information (Figures S5 and S6, Tables

Analysis of the data for this bulk sample suggest that around 19% is a species containing IS and QS values similar to that obtained for $[Fe^{II}(L^{\bullet})_2][BF_4]_2$[17] and so likely to contain a low-spin Fe(II) ion.

As seen in Scheme 1 (*vide-infra*), the electrochemical studies reveal a number of processes showing that $[Fe^{III}(L^-)_2]^+$ exists in equilibrium with $[Fe^{II}(L^{\bullet})(L^-)]^+$ and that $[Fe^{II}(L^{\bullet})_2]^{2+}$ is in equilibrium with $[Fe^{III}(L^{\bullet})(L^-)]^{2+}$ in acetonitrile solution. Thus, it is feasible that the second species could contain a combination of any of these cations in combination with the BF_4, $TCNQF_4\bullet$- or $TCNQF_4^{2-}$ anions. In our previous study on $[Fe^{III}(L^-)_2][BPh_4]$[17] we found no evidence of any second species in the Mössbauer spectrum, but electron paramagnetic resonance (EPR) studies on $[Fe^{II}(L^{\bullet})_2][BF_4]_2$[17] showed a small percentage (5% using a spin comparison with $CuSO_4 \cdot 5H_2O$) of a second minor species thought to be $[Fe^{III}(L^{\bullet})(L^-)]^{2+}$ which is in equilibrium with the $[Fe^{II}(L^{\bullet})_2]^{2+}$ dication. It is possible, therefore, that the monocation $[Fe^{III}(L^-)_2]^+$ can exist in equilibrium in the solid state with the $[Fe^{II}(L^{\bullet})(L^-)]^+$ monocation.

Data obtained by X-Ray Power diffraction studies on **1** are compared with those calculated from single crystal data for **1** and $[Fe^{II}(L\bullet)_2][BF_4]_2$ (Figures S1 and S2) to check for bulk phase purity of $[Fe^{III}(L^-)_2][TCNQF_4^{\bullet-}]$ (**1**) The resultant powder diffraction pattern at 298 K matches well with the theoretical powder diffraction pattern obtained from the CIF file for $[Fe^{III}(L^-)_2][TCNQF_4^{\bullet-}]$ (**1**) with no evidence of a second phase. This could be because any second species may be amorphous or simply lost in the signal to noise ratio

In summary, we have considered multiple scenarios to explain both the magnetic behavior of **1** and the nature of a 19% second minor species as evidenced by Mössbauer spectroscopy. The most likely option would suggest that **1** consists of 81% of the major species, $[Fe^{III}(L^-)_2][TCNQF_4^{\bullet-}]$, and 19% of a minor second species containing a central low-spin Fe(II) ion like the previously reported species, $[Fe^{II}(L^{\bullet})_2](BF_4)_2$.[17] The rise in the $\chi_M T$ value above 160 K is then accounted for by an observable antiferromagnetic coupling between the $[TCNQF_4]^{\bullet-}$ radical anions. This is favoured over any potential thermally induced spin-crossover transition of the $[Fe^{III}(L^-)_2]^+$ cation in **1**.

Solution Phase Studies on Dissolved Bulk Solid

Electrochemistry: With both the cation and anion in **1** being relatively easy to reduce and oxidize (Scheme 1), this material is expected to exhibit rich electrochemistry which should allow the thermodynamics of the numerous electron transfer processes and their interrelationships to be established in the solution phase.

The electrochemical behavior of a bulk sample of 0.6 mM **1** dissolved in CH_3CN (0.1 M Bu_4NPF_6) was studied initially by cyclic voltammetry at a glassy carbon macroelectrode. Under these transient conditions and over the potential range of -0.2 to 1.2 V vs Ag/Ag$^+$ a cyclic voltammogram of **1** exhibits four well-separated, diffusion controlled, one-electron, reversible processes labeled as I, II, III and IV in Figure 9. Processes I and

III are associated with the electrochemistry of the $TCNQF_4^{\bullet-}$ anion and II and IV with the that of the nitroxide based cation The mid-point potentials of these processes are $E_{mI} = 0.003$ V
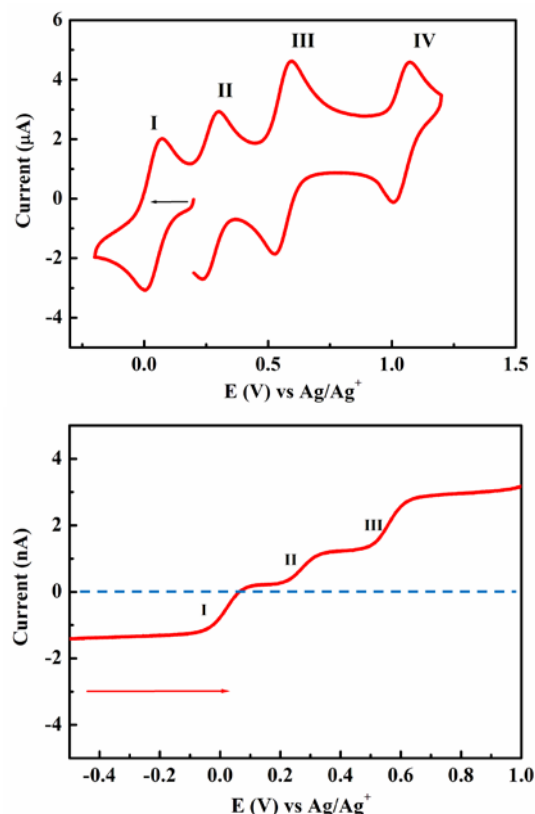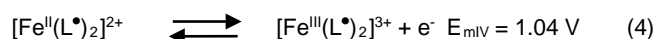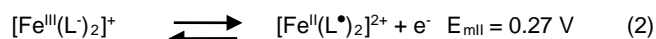

Figure 9. (top) Transient cyclic voltammogram of 1 at a glassy carbon disc macroelectrode obtained at a scan rate of 100 mV s^{-1}. (bottom) Steady-state voltammogram of 1 obtained at a Pt disc microelectrode. The solvent system in both cases is CH_3CN (0.1M Bu_4NPF_6).
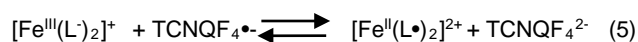
and $E_{mII} = 0.27$ V, $E_{mIII} = 0.56$ V and $E_{mIV} = 1.04$ V (vs Ag/Ag$^+$), where E_m is the average of the reduction (E_p^{red}) and oxidation (E_p^{ox}) peak potentials and represents a close approximation of the reversible formal potential $E^0{}_f$. The separation in the potentials ($\Delta Ep = Ep^{ox} - Ep^{red}$) for the four processes is similar to that obtained for the reversible oxidation of ferrocene, under the same conditions ($\Delta Ep = 62 - 65$ mV at a scan rate of 100mV s^{-1}), implying that all processes are electrochemically reversible under slow scan rate conditions.

The steady-state voltammogram for **1** at a Pt microelectrode is shown in Figure 9 over the potential range of -0.6 to +1.0 V vs Ag/Ag$^+$ where processes I, II and III were detected by the transient cyclic voltammetric method. (process IV is not covered by this experiment in the figure displayed, but is present in steady state ones covering a wider positive potential range). The half-wave potentials ($E_{1/2}$) calculated as the potential corresponding to the total limiting current (I_L) values are identical to E_m values from cyclic voltammetry as expected for reversible reactions and also consistent with literature values for independently prepared solutions of $TCNQF_4$ and $[Fe^{III}(L^-$
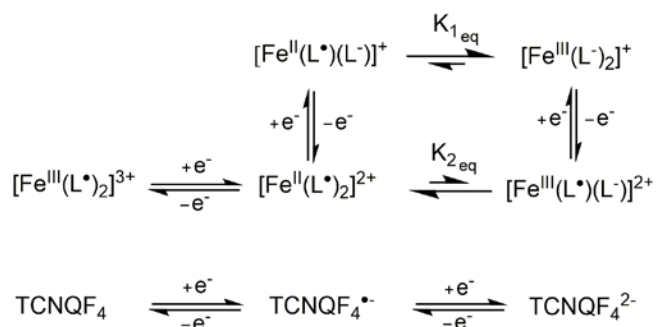
)$_2$]$^+$.[24,40] Most importantly, the potential range used in this experiment shown in Figure 9 was selected to cover the region that allows the position of zero current to be established, which then allows processes I to IV to be assigned as reductive or oxidative. Process I exhibits predominantly negative current, that is reduction current, but does contain a small component of positive or oxidation current consistent with the presence of a small concentration of TCNQF$_4$$^{2-}$. The major reductive component is assigned to a one-electron reduction of the TCNQF$_4$$^{•-}$ radical anion to the TCNQF$_4$$^{2-}$ dianion as in equation 1 and the small (about 15%) assigned to the reverse oxidation reaction (reverse of Eq. 1). Processes II-IV exhibit positive, that is oxidation, currents. Based on our voltammetric studies on [Fe^{II}(L$^-$)$_2$](BF$_4$)$_2$ and [Fe^{III}(L$^-$)$_2$](BPh$_4$),[17] processes II and IV are attributed to a one –electron oxidation of the monoanionic oxazolidine-N-oxide ligand (L$^-$) to generate the mixed-valent dication (Eq. 2), and metal-based Fe^{II} to Fe^{III} (Eq. 3) conversions, respectively. Finally, process III corresponds to a one–electron oxidation of TCNQF$_4$$^{•-}$ to neutral TCNQF$_4$ (Eq. 4), at the potential expected on the basis of literature data.[40] This further confirms the presence of TCNQF$_4$$^{•-}$ species in solutions of **1**, which can be reduced to TCNQF$_4$$^{2-}$ yielding a negative current (process I) or oxidised to TCNQF$_4$^{0} giving a positive current (process III). Thus the overall electrochemistry of **1** over the potential range covered by processes I to IV can be summarized by equations 1 to 4. Scheme 2 provides the full details of reactions associated with the square scheme summarized by the overall reaction in equation 2 along with a summary of the TCNQF$_4$$^{0/-/2-}$ redox chemistry. Process I (mainly reduction), process II (oxidation), process III (oxidation) and process IV (oxidation) are shown below:

$$TCNQF_4^{•-} + e^- \rightleftharpoons TCNQF_4^{2-} \qquad E_{mI} = 0.03 \text{ V} \qquad (1)$$

$$[Fe^{III}(L^-)_2]^+ \rightleftharpoons [Fe^{II}(L^•)_2]^{2+} + e^- \quad E_{mII} = 0.27 \text{ V} \qquad (2)$$

$$TCNQF_4^{•-} \rightleftharpoons TCNQF_4 + e^- \qquad E_{mIII} = 0.56 \text{ V} \qquad (3)$$

$$[Fe^{II}(L^•)_2]^{2+} \rightleftharpoons [Fe^{III}(L^•)_2]^{3+} + e^- \quad E_{mIV} = 1.04 \text{ V} \qquad (4)$$

The small concentration of TCNQF$_4$$^{2-}$ that can be oxidised to TCNQF$_4$$^{•-}$ implies that there is an equilibrium reaction as in equation 5 in acetonitrile or that the bulk sample contained some [Fe^{II}(L$^•$)$_2$][TCNQF$_4$$^{2-}$] which is a likely candidate for the second species present in bulk solid **1** detected by Mössbauer spectroscopy.

$$[Fe^{III}(L^-)_2]^+ + TCNQF_4^{•-} \rightleftharpoons [Fe^{II}(L^•)_2]^{2+} + TCNQF_4^{2-} \quad (5)$$

At more negative potentials than considered to date, and on the basis of the electrochemistry of [Fe^{II}(L$^•$)$_2$]$^{2+}$ (BF$_4$$^-$ as the counter cation) which is reduced to [Fe^{III}(L$^-$)$_2$]$^+$ at negative potentials and of [Fe^{III}(L$^-$)$_2$]$^+$ (BPh$_4$$^-$ as counter anion),[17] the Fe$^{(III)}$ $\rightleftharpoons$ Fe$^{(II)}$ metal based process given in equation 6 would

be expected to be detected at about -0. 8 V vs Ag/Ag+ for dissolved **1**.[17] However, while the more negative potential region does contain

Scheme 2. Square scheme and other redox processes involved in the electrochemistry of **1** (top) with K$_{1eq}$ and K$_{2eq}$ being relevant equilibrium constants and a summary of the different redox chemistry of TCNQF$_4$ (bottom).

this process V, it is present as a shoulder (Figure S4) on a multi-electron chemically reversible process VI which is followed by a minor process VII at even more negative potentials. Processes VI and VII are not seen when TCNQF$_4$$^{•-}$ is absent from the bulk solution. At these very negative potentials TCNQF$_4$$^{•-}$ has been reduced to TCNQF$_4$$^{2-}$ which itself is an excellent ligand.[41,42] Presumably, coordination and displacement of the nitroxide (L-) or rearrangement to a bidentate or monodentate form occurs leaving a new form of ligand that can be further reduced. Reduction to Fe(I) and an internal electron transfer reaction also may occur and square schemes analogous to reaction II could be operative. This nitroxide ligand based electroactivity introduces a very interesting difference created by the presence of TCNQF$_4$$^{2-}$ at the electrode surface, but insufficient information is available to warrant further speculation on the origin of processes VI and VII except for noting that the free nitroxide ligand radical (L$^•$) in CH$_3$CN (0.1 M [Bu$_4$N](PF$_6$)) can be irreversibly reduced[17] at -1.78 V vs Fc/Fc$^+$ or about -1.4 V vs Ag/Ag$^+$ which is similar to the potential for process VII.

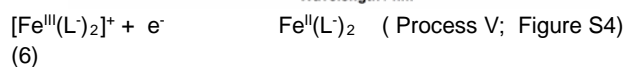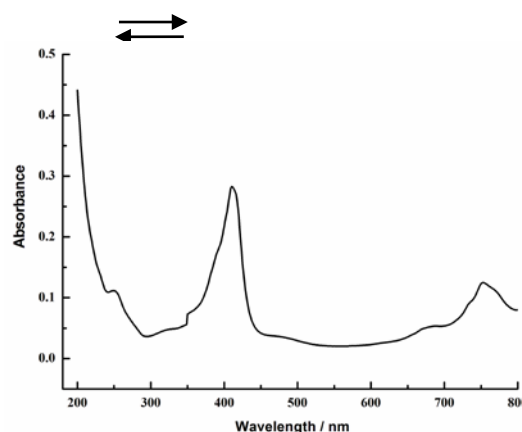$$[Fe^{III}(L^-)_2]^+ + e^- \rightleftharpoons Fe^{II}(L^-)_2 \quad (\text{Process V; Figure S4})$$
$$(6)$$

Figure 10. UV-vis spectrum for (top) approximately 0.1 mM **1** in acetonitrile.

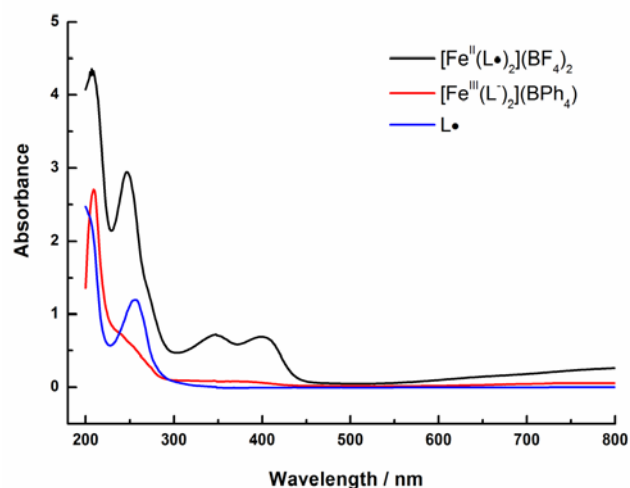**Figure 11.** UV-vis spectrum for 0.16 mM $[Fe^{II}(L\bullet)_2][BF_4]_2$ (black line) in acetonitrile with λ_{max} = 207, 247, 347 and 399 nm, 0.16mM $[Fe^{III}(L^-)_2](BPh_4).0.5H_2O$ (red line) in methanol with λ_{max} = 209, ~250 (shoulder) and 367 nm ~430 (shoulder) and 0.21 mM 4-dimethyl-2,2-di(2-pyridyl)oxazolidine-*N*-oxide (L•) in acetonitrile with λ_{max} = 257 nm.

Ultraviolet-visible spectroscopy: UV-vis spectra for **1** dissolved in acetonitrile (Figure 10) exhibit two strong absorption bands with λ_{max} at 752 and 411 nm which are characteristic for the $TCNQF_4^{\bullet-}$ radical anion [24,40] The weak absorption band at 251 nm for **1** is assigned to the monoanionic form of the ligand (L⁻) and its neutral radical form (L•) respectively (compare spectra in Figure 11). UV-vis spectra of $TCNQF_4$ and the one ($TCNQF_4^{\bullet-}$) and two electron ($TCNQF_4^{2-}$) reduced forms are available in reference 24, but resolution is inadequate to detect small concentrations of the dianion (or neutral $TCNQF_4$) in the presence of a considerably larger concentration of the anion radical or even if mixtures of L- and L• are present.

Conclusions

$[Fe^{III}(L^-)_2][TCNQF_4^{\bullet-}]$ (**1**) has been synthesized by the use of the $TCNQF_4^{2-}$ dianion in the form of Li_2TCNQF_4 which has effectively acted as a one electron reducing agent converting the $[Fe^{II}(L^\bullet)_2]^{2+}$ dication to $[Fe^{III}(L^-)_2]$ via a reductively induced oxidation. Structural and physical characterization of **1** reveals that the complex cation, $[Fe^{III}(L^-)_2]^+$, contains a central, and low-spin, Fe^{III} ion flanked by two ligands in their reduced form (L⁻) while the complex anion, $[TCNQF_4^{\bullet-}]$, is in the anionic radical form. The electrochemical studies revealed four distinct, reversible redox processes and additionally indicated the presence of a minor second species containing the $TCNQF_4^{2-}$

dianion. Mössbauer spectroscopy measurements provide more evidence of the presence of a minor second species, whose fitted parameters suggest the presence of a species similar to $[Fe^{II}(L^\bullet)_2](BF_4)_2$. Although there is a large number of possible cation and anion combinations, given the redox processes inherent in both, the most likely option for this minor second species is $[Fe^{II}(L^\bullet)_2][TCNQF_4^{2-}]$. The propensity of $TCNQF_4^{2-}$ to oxidise to its anionic radical form, $TCNQF_4^{\bullet-}$, means that potentially Li_2TCNQF_4 can be utilised as a driving force in the preparation of a series of cation/anion combinations, especially when the reduced form of a cation of choice may be more attractive from a materials chemistry perspective.

Experimental Section

General 4,4-dimethyl-2,2-di(2-pyridyl)oxazolidine-*N*-oxide (L•) and $[Fe^{II}(L^\bullet)_2][BF_4]_2$ were synthesized as described previously.[17–21] Li_2TCNQF_4 was prepared according to literature methods.[24] All other reagents and solvents were of reagent grade and used as received.

Syntheses. *$[Fe^{III}(L^-)_2][TCNQF_4^{\bullet-}]$ (1).* 24 mg (0.03 mmol) of $[Fe^{II}(L^\bullet)_2][BF_4]_2$¹ was dissolved in a solution containing 4 ml of acetonitrile and 1 ml of dichloromethane. This was then layered with a 1 ml methanolic solution containing 9.0 mg (0.03 mmol) of Li_2TCNQF_4. Green crystals suitable for X-Ray analysis formed after three days (16 mg, 59 % based on $[Fe^{II}(L^\bullet)_2][BF_4]_2$). FTIR (ATR cm⁻¹): $\tilde{v}$ = 2194s, 2174s, 1604m, 1531s, 1498s, 1465m, 1362w, 1343m, 1335s, 1294w, 1275w, 1224w, 1199m, 1167w, 1151w, 1142s, 1079m, 1057m, 996m, 965s, 938w, 904w, 877w, 784s, 768, 713w, 685m, 667m, 656s. Elemental analysis calculated (%) for $C_{42}H_{32}N_{10}O_4F_4Fe$ (**1**) : C 57.8, H 3.7, N 16.1; found: C 57.3, H 3.7, N 15.9. Raman spectra and X-ray powder diffraction patterns for **1** can be found in Figure 6 and Figures S1 and S2.

X-ray Crystallography. X-ray crystallographic measurements on **1** were undertaken at 123(2) K using a Bruker Smart Apex X8 diffractometer with Mo-Kα radiation (λ = 0.7107 Å). Single crystals were mounted on a glass fibre using oil for the data collection. Crystallographic data and refinement parameters for **1** are given in Table 5,were solved by direct methods (SHELXS-97), and refined (SHELXL-97) by full least-squares on all F^2 data.[43,44] In **1** the asymmetric unit contains half the iron monomer and half the $TCNQF_4^{\bullet-}$monoanion. For **1** all the non-hydrogen atoms were refined anisotropically and all hydrogen atoms placed in calculated positions. Full crystallographic data are available from the Cambridge Crystallographic Data Centre, 12 Union Road, Cambridge CB2 1EZ, UK. (http://www.ccdc.cam.ac.uk/). CCDC number of **1** is 1508567.

Powder X-ray Diffraction. Powder X-ray diffraction (PXRD) data were collected with a Bruker D8 Focus powder diffractometer using a scan step size of 0.01° at a rate of 2° min⁻¹. Calculated patterns from single crystal data were obtained using Mercury software.

Electrochemistry. Voltammetric experiments in a standard three - electrode cell were conducted at 22 ± 2 °C with a

Bioanalytical Systems BAS100B electrochemical workstation using a 0.6 mM solution of **1** in CH_3CN (0.1 M Bu_4NPF_6). The working electrode (WE) was either a glassy carbon macroelectrode (1 mm diameter, Bioanalytical Systems) or a Pt microelectrode (10 µm, Cypress). A platinum wire was used as the counter electrode. A silver wire immersed in acetonitrile solution containing 1.0 mM $AgNO_3$ and 0.1 M Bu_4NPF_6 was used as an Ag/Ag^+ reference electrode (RE) (the potential is 0.366 V vs Fc/Fc^+ couple, where Fc = ferrocene). Potentials are

Table 5. Crystallographic data for **1**

Parameters	**1**
Formula	$C_{42}H_{32}N_{10}O_4F_4Fe$
M_r	872.63
Crystal System	triclinic
Space Group	$P\bar{1}$
a /Å	8.0787(6)
b /Å	9.8244(8)
c /Å	11.9592(10)
α /°	89.534(2)
β /°	84.967(2)
γ /°	88.242(2)
V / Å^3	945.06(13)
T / K	123(2)
Z	1
ρ_{calcd} / g cm^{-3}	1.533
$\lambda^{[a]}$ / Å	0.71073
Ind. reflns	5121
Reflns with $I > 2\sigma(I)$	4131
Parameters	279
Restraints	0
Final $R1$, $wR2^{[b]}$ [$I > 2\sigma(I)$]	0.0433, 0.1034
$R1$, $wR2^{[b]}$ all data	0.0590, 0.1147
Goodness of fit	1.034
Largest residuals/ e Å^{-3}	0.479, -0.486

[a] Graphite monochromator. [b] $R1 = \Sigma | |F_o| - |F_c| | / \Sigma |F_o|$, $wR2 = \{\Sigma[w(F_o^2 \Sigma F_c^2)^2]/\Sigma[w(F_o^2)]\}^{1/2}$.

reported vs. the Ag/Ag^+ reference electrode. All solutions were degassed with nitrogen for 10 min prior to electrochemical experiments.

Infrared and Raman Spectroscopy. FTIR spectra were recorded using a Spectrac Diamond ATR instrument. Raman spectra were acquired with a Renishaw Raman RM2000 spectrometer and microscope using a laser strength of 18mW at a wavelength of 514 nm.

UV-Vis absorption spectroscopy. UV-vis spectra were recorded with a Varian Cary 5000 UV-vis NIR spectrophotometer on solutions contained in a 1.0 cm path length cuvette.

Mössbauer spectroscopy. A sample of **1**, as a slurry in Vaseline, was sealed into a Perspex holder. A room temperature Mössbauer spectrum was measured using a $^{57}CoRh$ source on a conventional constant acceleration spectrometer. Calibration and isomer shift reference both used an α-Fe absorber at room temperature.

Magnetic Susceptibility Measurements. Variable-temperature magnetic susceptibility measurements were performed on a Quantum Design MPMS 7T SQUID magnetometer over the temperature range 2 to 340 K and in an applied DC field of 0.5T. The SQUID magnetometer was calibrated by use of a standard palladium sample (Quantum Design) of accurately known magnetization or by use of magnetochemical calibrants such as $CuSO_4 \cdot 5H_2O$. Microcrystalline samples were dispersed in Vaseline in order to avoid torquing of the crystallites. The sample mulls were contained in a calibrated capsule held at the centre of a drinking straw that was fixed at the end of the sample rod.

Acknowledgements

[1]   K. Senthil Kumar, M. Ruben, *Coord. Chem. Rev.* **2017**, *346*, 176–205.
[2]   J. Martínez-Lillo, J. Faus, F. Lloret, M. Julve, *Coord. Chem. Rev.* **2015**, *289–290*, 215–237.
[3]   C. Bellitto, E. M. Bauer, G. Righini, *Coord. Chem. Rev.* **2015**, *289–290*, 123–136.
[4]   C. Sanchez, K. J. Shea, S. Kitagawa, *Chem. Soc. Rev.* **2011**, *40*, 696–753.
[5]   C. J. Kepert, *Chem. Commun. (Camb).* **2006**, 695–700.
[6]   E. Coronado, Galán-Mascarós José R., *J. Mater. Chem.* **2005**, *15*, 66.
[7]   S. Kitagawa, R. Kitaura, S. Noro, *Angew. Chemie - Int. Ed.* **2004**, *43*, 2334–2375.
[8]   E. Coronado, P. Day, *Chem. Rev.* **2004**, *104*, 5419–48.
[9]   D. Maspoch, D. Ruiz-Molina, J. Veciana, *J. Mater. Chem.* **2004**, *14*, 2713.

[10]   O. Sato, *Acc. Chem. Res.* **2003**, *36*, 692–700.

[11]   A. Abhervé, M. Clemente-León, E. Coronado, C. J. Gómez-García, M. Verneret, *Inorg. Chem.* **2014**, *53*, 12014–26.

[12]   Y. Murashima, M. R. Karim, N. Saigo, H. Takehira, R. Ohtani, M. Nakamura, M. Koinuma, L. F. Lindoy, K. Kuroiwa, S. Hayami, *Inorg. Chem. Front.* **2015**, *2*, 886–892.

[13]   K. Fukuroi, K. Takahashi, T. Mochida, T. Sakurai, H. Ohta, T. Yamamoto, Y. Einaga, H. Mori, *Angew. Chemie - Int. Ed.* **2014**, *53*, 1983–1986.

[14]   M. Clemente-León, E. Coronado, C. J. Gómez-García, M. López-Jordà, A. Camón, A. Repollés, F. Luis, *Chem. - A Eur. J.* **2014**, *20*, 1669–1676.

[15]   A. Lauria, I. Villa, M. Fasoli, M. Niederberger, A. Vedda, *ACS Nano* **2013**, *7*, 7041–52.

[16]   A. Tanushi, T. Kusamoto, Y. Hattori, K. Takada, H. Nishihara, *J. Am. Chem. Soc.* **2015**, *137*, 6448–6451.

[17]   I. A. Gass, C. J. Gartshore, D. W. Lupton, B. Moubaraki, A. Nafady, A. M. Bond, J. F. Boas, J. D. Cashion, C. Milsmann, K. Wieghardt, et al., *Inorg. Chem.* **2011**, *50*, 3052–3064.

[18]   S. Tewary, I. A. Gass, K. S. Murray, G. Rajaraman, *Eur. J. Inorg. Chem.* **2013**, *2013*, 1024–1032.

[19]   I. A. Gass, S. Tewary, A. Nafady, N. F. Chilton, C. J. Gartshore, M. Asadi, D. W. Lupton, B. Moubaraki, A. M. Bond, J. F. Boas, et al., *Inorg. Chem.* **2013**, *52*, 7557–7572.

[20]   I. A. Gass, S. Tewary, G. Rajaraman, M. Asadi, D. W. Lupton, B. Moubaraki, G. Chastanet, J.-F. Letard, K. S. Murray, *Inorg. Chem.* **2014**, *53*, 5055–5066.

[21]   I. A. Gass, M. Asadi, D. W. Lupton, B. Moubaraki, A. M. Bond, S.-X. Guo, K. S. Murray, *Aust. J. Chem.* **2014**, *67*, 1618.

[22]   P. W. Anderson, P. A. Lee, M. Saitoh, *Solid State Commun.* **1973**, *13*, 595–598.

[23]   X. Zhang, Z.-X. Wang, H. Xie, M.-X. Li, T. J. Woods, K. R. Dunbar, *Chem. Sci.* **2016**, *7*, 1569–1574.

[24]   J. Lu, T. H. Le, D. A. K. Traore, M. Wilce, A. M. Bond, L. L. Martin, *J. Org. Chem.* **2012**, *77*, 10568–10574.

[25]   T. J. Emge, M. Maxfield, D. O. Cowan, T. J. Kistenmacher, *Mol. Cryst. Liq. Cryst.* **1981**, *65*, 161–178.

[26]   S. a. O'Kane, R. Clérac, H. Zhao, X. Ouyang, J. R. Galán-Mascarós, R. Heintz, K. R. Dunbar, *J. Solid State Chem.* **2000**, *152*, 159–173.

[27]   S. A. Baudron, C. Mézière, K. Heuzé, M. Fourmigué, P. Batail, P. Molinié, P. Auban-Senzier, *J. Solid State Chem.* **2002**, *168*, 668–674.

[28]   I. V. Jourdain, M. Fourmigue, F. Guyon, J. Amaudrut, *J. Chem. Soc., Dalt. Trans.* **1998**, 483–488.

[29]   A. L. Sutton, B. F. Abrahams, D. M. D'Alessandro, T. A. Hudson, R. Robson, P. M. Usov, *CrystEngComm* **2016**, *18*, 8906–8914.

[30]   T. J. Emge, D. O. Cowan, A. N. Bloch, T. J. Kistenmacher, *Mol. Cryst. Liq. Cryst.* **1983**, *95*, 191–207.

[31]   T. Murata, G. Saito, K. Nakamura, M. Maesato, T. Hiramatsu, Y. Yoshida, *Cryst. Growth Des.* **2013**, *13*, 2778–2792.

[32]   M. Fourmigue, V. Perrocheau, R. Clerac, C. Coulon, *J. Mater. Chem.* **1997**, *7*, 2235–2241.

[33]   T. H. Le, J. Lu, A. M. Bond, L. L. Martin, *Inorganica Chim. Acta* **2013**, *395*, 252–254.

[34]   N. L. Haworth, J. Lu, N. Vo, T. H. Le, C. D. Thompson, A. M. Bond, L. L. Martin, *Chempluschem* **2014**, *3217*, n/a-n/a.

[35]   T. H. Le, A. P. O'Mullane, L. L. Martin, A. M. Bond, *J. Solid State Electrochem.* **2011**, *15*, 2293–2304.

[36]   H. Oshio, E. Ino, I. Mogi, T. Ito, *Inorg. Chem.* **1993**, *32*, 5697–5703.

[37]   P. J. Kunkeler, P. J. van Koningsbruggen, J. P. Cornelissen, A. N. van der Horst, A. M. van der Kraan, A. L. Spek, J. G. Haasnoot, J. Reedijk, *J. Am. Chem. Soc.* **1996**, *118*, 2190–2197.

[38]   A. M. Madalan, H. W. Roesky, M. Andruh, M. Noltemeyer, N. Stanica, *Chem. Commun.* **2002**, 1638–1639.

[39]   F. E. Mabbs, D. J. Machinn, *Magnetism and Transition Metal Complexes*, Chapman And Hall, London, **1973**.

[40]   J. Lu, B. F. Abrahams, B. Winther-Jensen, L. L. Martin, A. M. Bond, *ChemCatChem* **2014**, *6*, 2345–2353.

[41]   B. F. Abrahams, R. W. Elliott, T. A. Hudson, R. Robson, *Cryst. Growth Des.* **2013**, *13*, 3018–3027.

[42]   B. F. Abrahams, R. W. Elliott, T. A. Hudson, R. Robson, A. L. Sutton, *Cryst. Growth Des.* **2015**, *15*, 2437–2444.

[43]   G. M. Sheldrick, *SHELXL-97, Program for the Refinement of Crystal Structures*, University of Göttingen, Germany, **1997**.

[44]   A. L. Spek, IUCr, *Acta Crystallogr. Sect. A Found. Crystallogr.* **1990**, *46*, 34.

Entry for the Table of Contents (Please choose one layout)

Layout 1:

FULL PAPER

Li_2TCNQF_4 reduces the $[Fe^{II}(L^\bullet)_2]^{2+}$ dication found in $[Fe^{II}(L^\bullet)_2](BF_4)_2$ which then undergoes a reductively induced oxidation to form the $[Fe^{III}(L^-)_2]^+$ monocation resulting in the spontaneous redox formation of $[Fe^{III}(L^-)_2][TCNQF_4^{\bullet-}]$ ($L^\bullet$ / L^- are the neutral radical and hydroxylamino anionic form of the neutral radical chelating ligand, 4,4-dimethyl-2,2-di(2-pyridyl)oxazolidine-N-oxide).
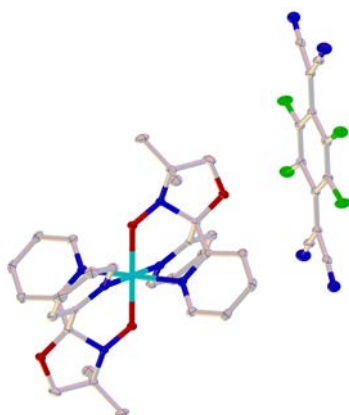
Ian A. Gass,* Jinzhen Lu] Mousa Asadi] David W. Lupton, Craig. M. Forsyth, Blaise L. Geoghegan, Boujemaa Moubaraki, John D. Cashion, Lisandra L. Martin,[a] Alan M. Bond,[a] and Keith S. Murray*[a]Author(s), Corresponding Author(s)*

Page No. – Page No.

The use of the $TCNQF_4^{2-}$ dianion in the spontaneous redox formation of $[Fe^{III}(L^-)_2][TCNQF_4^{\bullet-}]$.